International Journal of Innovative Technology and Exploring Engineering (IJITEE)
ISSN: 2278-3075 (Online), Volume-10 Issue-5, March 2021

Image Registration and Fusion using Moving Frame based Decomposition Framework Algorithm

Pooja Aspalli, Pattan Prakash

Abstract: ***Image fusion is an important process in the medical image diagnostics methods. Fusing images by obtaining information from different source and different types of images(modals) called multi-modal image fusion. This paper implements an effective and fast spatial domain based multi-modal image fusion using moving frame based decomposition (MFDF)method. Images from two different modalities are taken and decomposed to texture and approximation components. Weight mapping strategy is applied along with the guide filtering to fuse the approximation components using the final map. Weight mapping using the guide filtering is used for the fusing the images from different modalities. MATLAB is used for algorithm implementation. The results obtained are comparatively competitive with the recent publication[11]. Multi modal image fusion thus implemented gives promising results, when compared to moving frame decomposition framework method. The size and the blurring variable of the guiding filter is optimized to obtain a better Structural Similarity Index Measurement (SSIM).***

Keywords: Multimodal Image Fusion, Computer Tomography, Guide Filtering, Magnetic Resonance Imaging, Spatial domain image fusion.

I. INTRODUCTION

Image registration is an important pre-process step in image fusion, which helps to geometrically align two or more images. The image registration can be applied for fusion of medical images, satellite images or images obtained by different sensors at the same time or by same sensor at different times. This process involves designating one image as the reference image, also called the fixed image, and then applying geometric transformations or local displacements to the other images so that they align with the reference image. Images can be misaligned for various reasons. Generally images are captured under variable conditions that can change the camera perspective or the content of the scene. Basically, the registration of input images requires the selection of the feature space, a similarity measure or alignment quality, a transformation type and a search strategy. A great number of medical image registration methodologies have been presented, and several criteria have been proposed to classify them. by the data dimensionality (1D, 2D, 3D, 4D, …), source of the image features used to make the registration (intrinsic or extrinsic properties of patients), transformation domain (local or global), transformation elasticity (rigid, affine, projective or curved), tightness of property coupling (interpolating or approximating), parameter determination (direct or search-oriented), and interaction (interactive, semi-automatic or automatic).

Manuscript received on December 25, 2020.
Revised Manuscript received on January 08, 2021.
Manuscript published on March 30, 2021.

Pooja Aspalli*, Department of Computer Science and Engineering, PDA College of Vishveraya Technological University Kalaburagi

Dr. Prakash Pattan, Department of Computer Science and Engineering, P.D.A. College of Engineering, Gulbarga, Karnataka, India.

II. IMAGE REGISTRATION ALGORITHM CLASSIFICATION

Intensity Based Registration: The intensity-based registration methods operate directly on the image gray values, without reducing the gray-level image to relatively sparse extracted information. The basic principle of intensity-based techniques is to search, in a certain space of transformations, the one that maximizes (or minimizes) a criterion measuring the intensity similarity of corresponding voxels. Some measures of similarity are sum of squared differences in pixel intensities ([18]), regional correction [18], or mutual information ([19]). Mutual information has proved to be an excellent similarity measure for cross-modality registrations, since it assumes only that the statistical dependence of the voxel intensities is maximal when the images are geometrically aligned. The intensity similarity measure, combined with a measure of the structural integrity of the deforming scan, is optimized by adjusting parameters of the deformation field.Feature based Registration: Feature-based approaches attempt to find the correspondence and transformation using distinct anatomical features that are extracted from images Feature-based methods are typically applied when the local structure information is more significant than the information carried by the image intensity. They can handle complex between-image distortions and can be faster, since they don't evaluate a matching criterion on every single voxel in the image, but rather rely on a relatively small number of features. The simplest set of anatomical features is a set of landmarks. However, the selection of landmarks is recognized to be a difficult problem, whether done automatically or manually. For many images, this is a serious drawback because registration accuracy can be no better than what is achieved by the initial selection of landmarks. For practical reasons, the number and precision of landmark locations is usually limited. Hence, spatial coordinates and geometric primitives often oversimplify the data by being too sparse and imprecise. Image registration is often used as a preliminary step in various image processing applications. Image registration enables to compare common features in different images. Intensity based automatic image registration is an iterative process. It requires that you specify a pair of images, a metric, an optimizer and a transformation type. The metric defines the image similarity metric for evaluating the accuracy of the registration.

This image similarity metric takes two images and return a scalar value that describes how similar the images are. The optimizer defines the methodology for minimizing or maximizing the similarity metric.

The transformation type defines the type of 2D transformation that aligns the misaligned image(called the moving image) with the reference image(called the fixed image). The process begins with the transform type you specify and an internally determined transformation matrix. Together they determine the specific image transformation that is applied to the moving image with bilinear interpolation. Next, the metric compares the transformed moving image to the fixed image and a metric value is computed. Image fusion methods are classified as single and multimodal based image fusion methods.

The Computer Tomography (CT) and Magnetic Resonance Imaging (MRI) are the most preferred for medical diagnosis. Advanced imaging modalities like by positron emission tomography (PET) and single photon emission (SPECT) are used to obtain images of metabolism of organisms. Each imaging modality highlight different information in the diagnosis process. Important characteristics of the fused images are, information from the source image is retained completely, synthetic information like artefacts should not be created, noise and misregistration should be avoided [1]. Image fusion methods are further classified as spatial and transform based image fusion methods. At the image level, the fusion is at pixel level, signal, feature and symbol level. Pixel level method adopts transform domain-based image fusion implementation. These methods apply image transformation and the fusion is applied in the transform domain. Advantage of the transform domain is that it provides noise filtering and maintain good structure [2-3] Implementing both the transform domain and the spatial domain algorithm is used for fusing images. PCA-DWT method is applied that improves the image structure and avoid artefacts [4]. Transform based methods acts as a filter that smooth the image in both spatial and spectral level. Contourlet transformation is advantageous to the wavelet transform in removing the artifacts [5]. Image distortion is evident at the singular point of the reconstructed images. An advanced contourlet algorithm is developed. The distortion removal is evident in the implementation. A smooth decomposition and reconstruction are evident in the advanced contourlet developed [6].

Log Gabor frequency sub bands are combined with a interpolated weighing to get the fused image [7].The weighing strategy is developed using the type-2 fuzzy logic algorithm. Sparse representation-based image fusion methods that adjust the basis vectors of the image to obtain a better fused image is carried out. It is applied on the multimodal images [8]. Nonsubsampled Contourlet Transform (NSCT) is used with Darwinian particle swarm optimization (DPSO) for image fusion. DPSO selects the features from the NSCT domain for the image and combines it for image fusion. A multimodal image fusion is applied on the images using the pulse-coupled neural network algorithm (PCNN) and the NSCT domain. Sparse representation and PCNN are combined to model the image fusion algorithm [10].

This paper implements the multimodal image fusion algorithm in the spatial domain, Spatial domain methods work by combining the pixel values of the two or more images to be fused in a linear or nonlinear way, the simplest form is a Weighted Averaging method due to which it is inferred that spatial method is a novel method to carry out this research work. MFDF algorithm is implemented to decompose the images under study and the image fusion is carried out. The rest of the paper is organised as follows, Section 2 discusses about the MFDF algorithm, Section 3 discusses about the results and discussions obtained from the algorithm.

III. METHODOLOGY

2.1 Moving Frame based Decomposition Framework

The performance analysis of the fusion method defined in [11] is implemented using the following steps.

1. Unlike the multiscale transform-based image fusion technique this technique uses only the single level transformation. The selection of decomposition levels of the transformation technique is not decided.
2. Image properties and guided filters decides the weight map using refining strategy. These weight map helps in fusing the images with approximation components.
3. A multimodal approach for image fusion thus carried out in the technique retains edge and texture information and at the same time with good contrast and relevant for human vision.

2.2 Detailed Fusion Scheme

There are three procedures involved in the MFDF decomposition. The detailed discussion of the procedures is discussed in the following paragraphs.

2.2.1.MFDF Decomposition:

MFDF method generates a matrix as defined in equation (1), where the parameter μ is a smoothing parameter for the moving frame encoding the local geometry of the original image. In the equation (1) the texture and the approximation components are discussed. Since fusion is multimodal in nature, hence two images Image A and Image B are used, which is the decomposition stage having texture and approximation components.

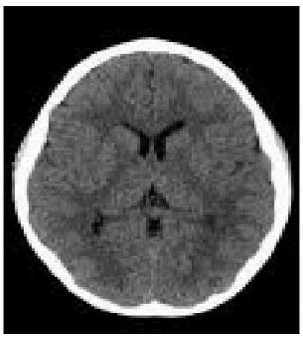

Image A: CT

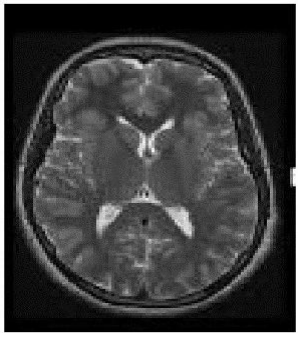

Image B: MRI

$$P = \begin{bmatrix} \frac{I_x}{|\nabla|\sqrt{1+\mu^2|\nabla I|^2}} & -\frac{I_y}{|\nabla|} & -\frac{\mu I_x}{\sqrt{1+\mu^2|\nabla I|^2}} \\ \frac{I_y}{|\nabla I|\sqrt{1+\mu^2}} & \frac{I_x}{|\nabla I|} & -\frac{\mu I_y}{\sqrt{1+\mu^2|\nabla I|^2}} \\ \frac{\mu|\nabla I|}{\sqrt{1+\mu^2|\nabla I|^2}} & 0 & \frac{1}{\sqrt{1+\mu^2|\nabla I|^2}} \end{bmatrix} \quad (1)$$

The moving frame is encoded by exploiting the local geometry. Smoothing parameter $\mu$for moving frame of the original image I. $\{A_T, A_A\}$and $\{B_T, B_A\}$ are the decomposed components of both A and B images.
Subscript 'T' defines the texture component while subscript 'A' defines the approximation component.

2.2.2.Fusion of Texture Components:

Fused portion of the texture components F_T is generated by using the 'max-absolute' rule. This rule is applied on the texture components of both the images A_T *and* B_T. In order to ensure participation of both the images in the fused image the consistency verification using a majority filter is applied as defined in equation (2) and (3).

$$MAX_A = MAJORITY(abs(A_T), W) \quad (2)$$

$$MAX_B = MAJORITY(abs(B_T), W) \quad (3)$$

$$mm = \left((MAX_A > MAX_B) * W\right) > floor(r \times r/2) \quad (4)$$

$$F_T = mm.\times A_T + \left((\sim mm).B_T\right) \quad (5)$$

Equation (4) and (5) defines the fusion implementation of the texture components. In the equations (2)-(5), majority represents the majority filtering operation in the window W, the size of which is r×r.

2.2.3.Fusion of Approximation Components:

The approximation components of the images are filtered using both the Laplacian and Gaussian filter to obtain the components S_A and S_B. Equation (6) and (7) defines these components.

$$S_A = Gau(Lap(A_A, W_t), W_{gr,g\sigma} \quad (6)$$

$$S_B = Gau(Lap(B_A, W_t), W_{gr,g\sigma} \quad (7)$$

Where Lap is Laplacian filter and Gau represents the Gaussian filtering. The window size W_t is 3X3. Using these components, the mapping P_A and P_B are developed using the equation (12) and (13).$W_{gr,g\sigma}$ of size $(2g_r + 1) \times (2g_r + 1)$ and the parameter g_r *and* σ_r are set the same values.

$$P_A = S_A > S_B \quad (8)$$

$$P_B = S_A < S_B \quad (9)$$

The map obtained from equation (8) and (9) are segmented using the threshold value. Thresholds defined in equation (10) and (11) is defined as th1 and th2 for two images. This threshold is calculated by finding the mean of the first 5%-pixel values original images.

$$w_1 = Thsegment(A_A, th1) \quad (10)$$

$$w_2 = Thsegment(B_A, th2) \quad (11)$$

Segmented images w_1 *and* $w_2$of both the images A and B are further filtered using the guide filter as discussed in equation (12) and (13).

$$T_A = GF_{r,\epsilon}\left(((P_A|w_1)\&(\sim w_2)), A_A\right) \quad (12)$$

$$T_B = GF_{r,\epsilon}\left(((P_B|w_2)\&(\sim w_1)), B_A\right) \quad (13)$$

Where $GF_{r,\epsilon}$ represents the guide filtering operation, and the parameters r *and* ϵ set to 4 and 0.3. The subscript r is the size and ϵ is the blurring constant of the guiding filter.
Note that the segmentation procedure is essential in refining the final mapwhich shows the effectiveness of the segmentation procedure in the computation of T_A *and* T_B. The computation of T_A *and* $T_B$without the segmentation procedure can be expressed as formulas (14) and (15).

$$T_A = GF_{r,\epsilon}(P_A, A_A) \quad (14)$$

$$T_B = GF_{r,\epsilon}(P_B, B_A) \quad (15)$$

Finally, the fused approximation component F_A is obtained by the weight average of A_A *and* B_A with the final map T_A*and* T_B

$$F_A = T_A \times A_A + T_B \times B_A \quad (16)$$

The block diagram for the optimized MFDF that is adopted in the implementation is as shown in the below diagram

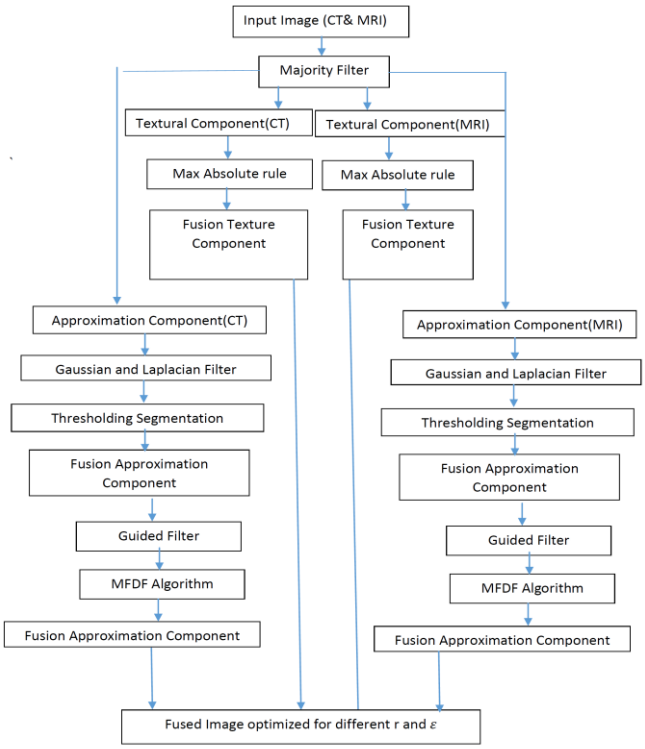

Fig 1: Block diagram of the Similarity Index Optimized Image Fusion using Moving Frame based Decomposition Framework Algorithm

IV. RESULTS AND DISCUSSIONS

Since the implementation is the multimodal image fusion framework medical images are chosen for testing. CT and MRI images are the two modalities chosen for the image fusion algorithm. Figure 2 shows the CT and MRI brain images used for the fusion process. The Fig (a) is the CT brain image taken for the fusion. The approximation and the texture components of the input CT image is as shown in Fig (b) and Fig (c) respectively.

The second image chosen for fusion is the MRI image, it is shown in Fig (d). The approximation components and the texture component of the chosen MRI image is shown in Fig (e)& Fig (f) respectively. Table 1 defines all the parameters that are used for the MFDF implementations on the CT and MRI images.

\

There are two sets of images that are been used for the implementation, one is the brain image and the other is the spine image.

Table 1. Methods used in Image Fusion Process

Sl. No	Methods	Notation	Values
01	Majority filtering operation in the window size	W	3
02	Laplacian filtering	W1(2,2)	8
03	Guide filtering operation parameters	R, ϵ	4(Size), 0.3(Constant)

Fig (a) Input CT image

Fig (b) Approximation Component

Fig (c): Texture component

Shown in Fig (a) Shown in Fig(a)

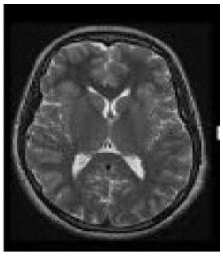

Fig (d) MRI input Image

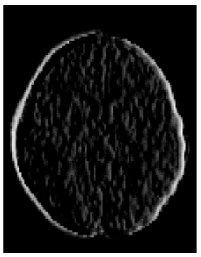

Fig (e)Texture Component

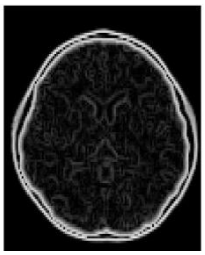

Fig(f) Approximation Component

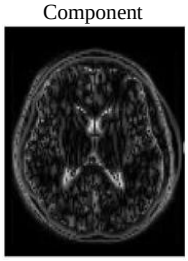

Fig(g) Fused Output

Fig 2: Fusion process of CT and MRI brain images: (a) CT input image (b) Texture Component of CT image (c) Approximation component of CT image (d) MRI input image (e) Texture component of MRI image (f) Approximation component of MRI image (g) Fused image.

After applying the MFDF algorithm defined in the above section the fused image is found using the following formula defined in equation (17).

$$F = \sqrt{F_T, \times F_T + F_A . \times F_A} \qquad (17)$$

The fused image obtained from the equation (17) is as shown in Fig (g). It is observed that the multimodal characteristics of both the CT and MRI images are intact in the fused image. Fusion output gets the major texture part of the input image and applied with Gaussian filtering. The approximation component is obtained from the gaussian filtering framework and guided filter provides the contribution of each modality. The following table 2 and 3 represents the MSE and SSIM values obtained from the image fusion of brain images.

Table 2. MSE obtained from the Image Fusion for brain image

Input Image	Fusion MSE (MFDF) Proposed Epsilon varying between 0.003 to 0.3 with .05 increment
CT actual image	0.0960 0.0966 0.0970 0.0973 0.0975 0.0977
MRI actual image	0.0623 0.0631 0.0637 0.0641 0.0645 0.0647

The (SSIM) for variation in the $\boldsymbol{\varepsilon}$during the fusion implementation is obtained in the Table 3.

Table 3. SSIM for variation in the ε for brain image

SSIM1 (MFDF) $\varepsilon = .3$, r=4	SSIM2 (MFDF) $\varepsilon = .3$, r=4	SSIM1 (optimized MFDF) $\varepsilon = .003$, r=1	SSIM2 (optimized MFDF) $\varepsilon = .003$, r=1
0.3128	0.4266	0.3384	0.4461

SSIM values obtained between the fused images and CT and MRI image is defined as SSIM1 and SSIM2 respectively. The increased value of SSIM clearly indicates that the fused image represents both the CT and MRI images in a very close manner. The Table 3 compares the MFDF method with the proposed work and results are discussed. The images used for this proposed method and comparison is given in [12].The proposed improvement in the implementation is applied by varying the eps and r value and it is found that the SSIM improves with the decrease in eps and r values. Table 4 depicts the SSIM values for varying values of r with a constant different values. In the Table 4SSIM1 stands for the CT images while SSIM2 stands for MRI images. It can be observed that the SSIM is higher for the values r=1 and eps=0.003.

Table 4. SSIM versus 'r' for Brain Images (CT—SSIM1, MRI-SSIM2)

Epsilon variation between 0.003 to 0.3						'r' variation	SSIM1-CT SSIM2-MRI
0.3213	0.3188	0.3168	0.3152	0.3139	0.3128	r=4	SSIM1
0.4357	0.4327	0.4305	0.4289	0.4276	0.4266		SSIM2
0.3001	0.2977	0.2960	0.2948	0.2938	0.2931	r=10	SSIM1
0.4133	0.4120	0.4112	0.4106	0.4101	0.4097		SSIM2
0.2936	0.2920	0.2909	0.2900	0.2894	0.2889	r=15	SSIM1
0.4079	0.4074	0.4070	0.4068	0.4066	0.4064		SSIM2
0.2908	0.2895	0.2886	0.2879	0.2874	0.2870	r=20	SSIM1
0.4053	0.4052	0.4050	0.4049	0.4048	0.4047		SSIM2
0.3253	0.3239	0.3226	0.3215	0.3206	0.3198	r=3	SSIM1
0.4406	0.4381	0.4362	0.4348	0.4336	0.4326		SSIM2
0.3299	0.3296	0.3292	0.3289	0.3285	0.3282	r=2	SSIM1
0.4439	0.4424	0.4412	0.4403	0.4395	0.4389		SSIM2
0.3384	0.3386	0.3387	0.3388	0.3388	0.3389	r=1	SSIM1
0.4461	0.4458	0.4455	0.4452	0.4450	0.4449		SSIM2

Next part of the research work is done by using the spine images.

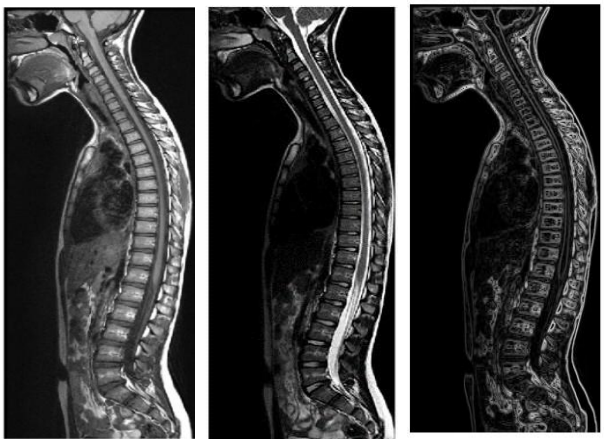

Fig(a) CT Input Image **Fig(b)Texture Component** **Fig(c)Approximation**

Shown in Fig (a) Shown in Fig

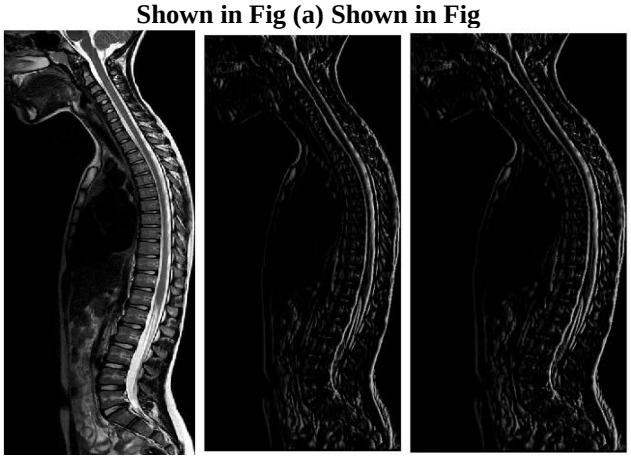

Fig (d) MRI image input **Fig(e)Texture component** **Fig(f).Approximation Component**

Fig (g). Fused Image

Fig 3: Fusion process of CT and MRI spine images: (a) CT input image (b) Texture Component of CT image (c) Approximation component of CT image (d) MRI input image (e) Texture component of MRI image (f) Approximation component of MRI image (g) Fused image.

After applying the MFDF algorithm defined in the above section the fused image is found using the following formula defined in equation (17).

$$F = \sqrt{F_T, \times F_T + F_A . \times F_A} \qquad (17)$$

Tabulated values of Mean Square Error (MSE) and Structural Similarity Index Measurement (SSIM) is obtained between the actual image and the corresponding original CT and MRI images. The values are shown in the Table 5 & 6 respectively. The image size of 328X328 images is applied in the proposed method.

Table 5. MSE obtained from the Image Fusionfor Spine image

Input Image	Fusion MSE (MFDF) Proposed Epsilon varying between 0.003to 0.3 with .05 increment
CT actual image	0.0390 0.0392 0.0393 0.0394 0.0395 0.0395
MRI actual image	0.0501 0.0504 0.0506 0.0507 0.0508 0.0509

The (SSIM) for variation in the εduring the fusion implementation is obtained in the Table 6.

Table 6. SSIM for variation in the ε and r for spine image

SSIM1 (MFDF) $\varepsilon = .3$, r=4	SSIM2 (MFDF) $\varepsilon = .3$, r=4	SSIM1 (Optimized MFDF) $\varepsilon = .003$, r=1	SSIM2 (Optimized MFDF) $\varepsilon = .003$, r=1
0.3541	0.2581	0.3724	0.2641

Table 7 depicts SSIM values obtained between the fused images and CT and MRI of spine image is defined as SSIM1 and SSIM2 respectively. The increased value of SSIM clearly indicates that the fused image represents both the CT and MRI images in a very close manner.

Table 7. SSIM for variation in the ε and r values for spine image

Epsilon variation between 0.003 to 0.3						'r' variation	SSIM1-CT SSIM2-MRI
0.3550	0.3546	0.3544	0.3543	0.3541	0.3541	r=4	SSIM1
0.2592	0.2589	0.2586	0.2584	0.2583	0.2581		SSIM2
0.3478	0.3477	0.3476	0.3475	0.3475	0.3474	r=10	SSIM1
0.2565	0.2563	0.2561	0.2559	0.2558	0.2557		SSIM2
0.3457	0.3457	0.3456	0.3456	0.3456	0.3456	r=15	SSIM1
0.2554	0.2551	0.2549	0.2547	0.2546	0.2545		SSIM2
0.3444	0.3444	0.3444	0.3444	0.3444	0.3444	r=20	SSIM1
0.2546	0.2542	0.2540	0.2538	0.2537	0.2536		SSIM2
0.3589	0.3584	0.3581	0.3579	0.3578	0.3576	r=3	SSIM1
0.2605	0.2601	0.2598	0.2595	0.2593	0.2592		SSIM2
0.3647	0.3641	0.3638	0.3635	0.3634	0.3632	r=2	SSIM1
0.2621	0.2616	0.2613	0.2611	0.2609	0.2607		SSIM2
0.3724	0.3719	0.3716	0.3714	0.3712	0.3711	r=1	SSIM1
0.2641	0.2638	0.2636	0.2634	0.2633	0.2632		SSIM2

The Table 6 compares the MFDF method with the proposed work and results are discussed. The images used for this proposed method and comparison is given in [12].It can be observed that the SSIM is higher for the values r=1 and eps=0.003.

The proposed improvement in theimplementation is applied by varying the ε and r value and it is found that the SSIM improves with the decrease in ε and r values.

The proposed improvement in theimplementation is applied by varying the ε and r value and it is found that the SSIM value is improved with the variation in ε and r values.Figure 4 represents the graph of brain images with eps versus SSIM1(CT image) and Figure 5 represents the graph with eps versus SSIM2(MRI image). And Figure 6 represents the graph of spine images with eps versus SSIM1(MRI image) and Figure 7 represents the graph with eps versus SSIM2(CT image).

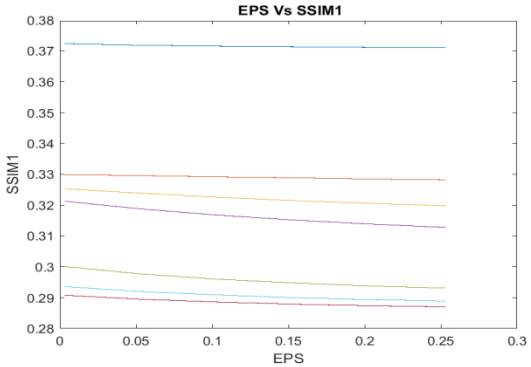

Fig 4: SSIM versus 'r' for brain Images(CT)

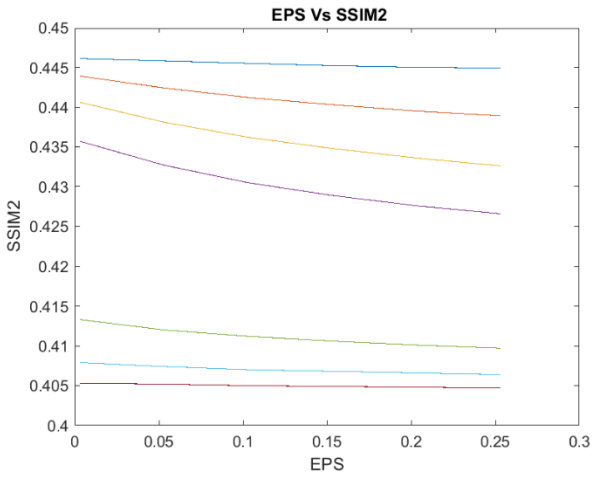

Fig 5 :SSIM versus 'r' for brain Images(MRI)

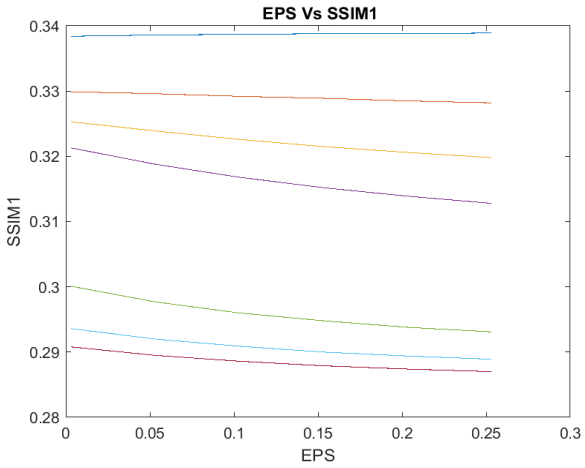

Fig 6 :SSIM versus 'r' for spine Images(MRI)

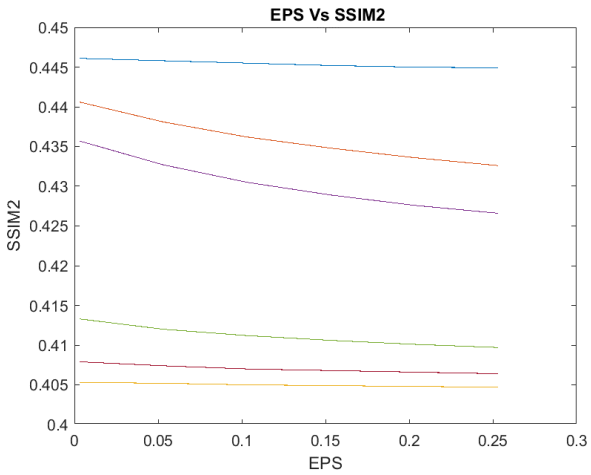

Fig 7: SSIM versus 'r' for spine Images(CT)

V. CONCLUSION

MATLAB based implementation on the MFDF based image fusion is developed. The results obtained from the MFDF technique provides an optimal guided filter value for a better image fusion.

The fused image obtained from the MFDF method provided better MSE and SSIM and is in terms with the recent publications. SSIM values obtained between the fused images and CT and MRI image is defined as SSIM1 and SSIM2 respectively. The increased value of SSIM clearly indicates that the fused image represents both the CT and MRI images in a very close manner.

REFERENCES

1. B. Meher, S. Agrawal, R. Panda, and A. Abraham, "A survey on region-based image fusion methods," *Information Fusion*, vol. 48, pp. 119–132, 2019.
2. W. Zhao and H. Lu, "Medical image fusion and denoising with alternating sequential filter and adaptive fractional order total variation," *IEEE Transactions on Instrumentation and Measurement*, vol. 66, no. 9, pp. 2283–2294, 2017.
3. N. Iqbal, S. Saleem, W. S. Jehan, and K. Ahmad, "Reduction of speckle noise in medical images using stationary wavelet transform and fuzzy logic," in *2017 International Symposium on Recent Advances in Electrical Engineering (RAEE)*, Islamabad, Pakistan, October 2017.
4. S. Madanala and K. Jhansi Rani, "PCA-DWT based medical image fusion using non sub-sampled contourlet transform," in *2016 International Conference on Signal Processing, Communication, Power and Embedded System (SCOPES)*, Paralakhemundi, India, October 2016.
5. M. N. Do and M. Vetterli, "The contourlet transform: an efficient directional multiresolution image representation," *IEEE Transactions on Image Processing*, vol. 14, no. 12, pp. 2091–2106, 2005.
6. A. L. da Cunha, J. Zhou, and M. N. Do, "The nonsubsampled contourlet transform: theory, design, and applications," *IEEE Transactions on Image Processing*, vol. 15, no. 10, pp. 3089–3101, 2006.
7. Y. Yang, Y. Que, S. Huang, and P. Lin, "Multimodal sensor medical image fusion based on type-2 fuzzy logic in NSCT domain," *IEEE Sensors Journal*, vol. 16, no. 10, pp. 3735–3745, 2016.
8. F. Shabanzade and H. Ghassemian, "Multimodal image fusion via sparse representation and clustering-based dictionary learning algorithm in nonsubsampled contourlet domain," in *2016 8th International Symposium on Telecommunications (IST)*, Tehran, Iran, September 2016.
9. Mahima, N. B. Padmavathi, and M. V. Karki, "Feature extraction using DPSO for medical image fusion based on NSCT," in *2017 2nd IEEE International Conference on Recent Trends in Electronics, Information & Communication Technology (RTEICT)*, pp. 265–269, Bangalore, India, May 2017
10. A. Mohammed, K. L. Nisha, and P. S. Sathidevi, "A novel medical image fusion scheme employing sparse representation and dual PCNN in the NSCT domain," in *2016 IEEE Region 10 Conference (TENCON)*, Singapore, Singapore, November 2016.
11. H. Yan and Z. Li, "A Multi-modal Medical Image Fusion Method in Spatial Domain," 2019 IEEE 3rd Information Technology, Networking, Electronic and Automation Control Conference (ITNEC), Chengdu, China, 2019, pp. 597-601, doi: 10.1109/ITNEC.2019.8729143.
12. http://www.med.harvard.edu/AANLIB/

AUTHORS PROFILE

Pooja Aspalli, born in the year 1989,completed her B.E degree in Computer Science and Engineering from PDA College of Engineering, Vishveraya Technological University Kalaburagi in 2011, M.Tech degree in Computer Science and Engineering from PDA College of Engineering, Vishveraya Technological University Kalaburagi in 2014, currently working as Asstiant Professor Computer Science and Engineering from PDA College of Engineering, Kalaburagi.

Dr. Prakash Pattan, System Manager (Professor), serving in Department of Computer Science and Engineering, P.D.A. College of Engineering, Gulbarga, Karnataka, India. He has obtained M.Sc. (Information Technology) degree in 2003 and M. Tech. (Information Technology) degree in 2006. He has completed Ph.D. from Jawaharlal Nehru Technological University, Hyderabad in 2014. His research areas of interest are; Image Processing, Computer Networking and Pattern Recognition. He has published more than 34 research papers in peer reviewed International Journals and Proceedings of Conferences. Currently he is guiding 7 research scholars for the award of Ph.D. His two research works are published in a reference book entitled "Measuring Shapes" authored by Dr. Jhon C. Russ, Tailor and Francis Press.